Computational Analysis of an Electro-Thermal Ice Protection System in Atmospheric Icing Conditions

L.P. Raj[1] and R.S. Myong[*1,2]

[1]Graduate School of Mechanical and Aerospace Engineering, Gyeongsang Nat'l Univ.
[2]Dept. of Aerospace and Software Engineering & Research Center for Aircraft Parts Technology, Gyeongsang Nat'l Univ.

대기 결빙 조건에서의 전기열 방식 결빙보호 시스템에 관한 전산해석

프린스 라즈,[1] 명 노 신[*1,2]

[1]경상대학교 대학원 기계항공공학부
[2]경상대학교 항공우주및SW공학전공 및 항공기부품기술연구소

Atmospheric icing may have significant effects not only on safety of aircraft in air, but also on performance of wind turbine and power networks on ground. Thus, ice protection measure should be developed to protect these systems from icing hazards. A very efficient method is the electro-thermal de-icing based on a process by which ice accretion is melted and blown away through aerodynamic forces. In this computational study, a state-of-the-art icing code, FENSAP-ICE, was used for the analysis of electro thermal de-icing system. Computational results including detailed conjugate heat transfer analysis were then validated with experimental data. Further, the computational model was applied to the DU21 airfoil section of NREL 5MW wind turbine with calculated heater parameters.

Key Words : Atmospheric Icing, CFD, Conjugate Heat Transfer, Ice Protection System

1. Introduction

The study of atmospheric icing effects on aircraft and wind turbine is of critical importance due to significant degradation of aerodynamic performance[1-7]. Accumulation of ice on the leading edge surfaces of aircraft and wind turbine blades will result in disruption of smooth flow, reduction of lift and increase of drag, stall at much higher speeds than normal, vibrations due to mass imbalance, and damage of aircraft or wind turbine components due to ice shedding[8-10].

Generally, ice accretion is caused by supercooled droplets in metastable state in the clouds. When droplets impact on the surface of aircraft or wind turbine blades, they may suddenly change phase and freeze on the surface. Normally, the temperature range of icing is from -40 to 0 C. Accumulated ice can be classified as rime, glaze or mixed. The shape and type of ice accretion depend on geometry, airspeed, mean volumetric diameter of the droplet(MVD), liquid water content of cloud (LWC), exposure time, surface roughness, and temperature.

Ice can accrete on different locations of aircraft and wind turbines. Nonetheless, the most critical locations are leading edges of the wings, empennages, propeller, engine inlets of aircraft and blades of wind turbines. Ice protection systems(IPS) are employed to enhance the aircraft flight safety and to avoid the loss of performance of wind turbines. The ice protection systems are based on the concept of anti-icing and de-icing. The former prevents the ice formation from the start, while the later removes the accreted ice layer before it causes significant degradation of performance. Various types of IPS have

been developed; pneumatic boot de-icing system, hot-air anti-icing system, weeping fluid system, electro mechanical expulsive de-icing systems(EMEDS) and electro-thermal de-icing system(ETDS). Among these systems, ETDS is the most effective method for aircraft and wind turbine applications[11,12], owing to the advantage of no bleed air required and high system efficiency achieved from local customization at each zone. Electro-thermal ice protection systems have already been used in helicopter blades and propellers and the main wing of the Boeing 787 transport aircraft.

Basically, electro-thermal de-icer has an electric heater placed under the wing surface or wind turbine blades. The challenge is to minimize power consumption while avoiding ridges on the upper surface of the wing and wind turbine blades. In this study, the analysis of electro-thermal ice protection system is conducted for NACA0012 airfoil using a state-of-the-art CFD code to validate the current computational model. The validated computational model is applied to a wind turbine blade section DU21.

2. Numerical Simulation of Electro-Thermal Ice Protection System

The simulation of electro-thermal ice protection system starts with the air flow computation around the airfoil. The compressible Navier-Stokes-Fourier code based on the finite volume method and the Roe's approximate Riemann solver, FLUENT, are used. A simple Spalart-Allmaras turbulence model is employed to compute turbulence effects in dry air. Riemann invariant is implemented for far-field boundary condition along with no slip boundary for solid surfaces.

Droplet impingement and ice accretion are simulated by DROP3D and ICE3D modules of the icing code FENSAP-ICE[13]. The DROP3D[14] module solves liquid water content and droplet velocities in an Eulerian framework and predicts the amount of water collected by the exposed surface. The ICE3D module determines the ice accretion and water runback in conjunction with the CHT3D module, the conjugate heat transfer module of FENSAP-ICE, based on the coupled heat convection and conduction equations.

The droplet impingement solver DROP3D is based on the finite element method and the Newton's method is used to linearize the non-linear governing equations. The continuity and momentum equations of Eulerian droplet

motion[15] can be written as,

$$\frac{\partial \alpha}{\partial t} + \nabla \cdot (\alpha \, \boldsymbol{u_d}) = 0 \tag{1}$$

$$\frac{D\boldsymbol{u_d}}{Dt} = \frac{C_D \, Re_d}{24K}(\boldsymbol{u_a} - \boldsymbol{u_d}) + \left(1 - \frac{\rho_a}{\rho_w}\right)\frac{1}{Fr^2}\boldsymbol{g} \\ + \frac{\rho_a}{\rho_w}\frac{D_a \boldsymbol{u_a}}{Dt} \tag{2}$$

where variables α and $\boldsymbol{u_d}$ are the mean values of non-dimensional water volume fraction and droplet velocity vector over a small fluid element around the location x at time t. The first term on the right-hand-side of the momentum equation represents the drag acting on droplets of mean diameter d. It is proportional to the relative droplet velocity, its drag coefficient C_d and the droplet Reynolds number,

$$Re_d = \frac{\rho_a d u_{a,\alpha} \parallel \boldsymbol{u_a} - \boldsymbol{u_d} \parallel}{\mu_a} \tag{3}$$

and an inertial parameter,

$$K = \frac{\rho_d d^2 \boldsymbol{u_{a,\alpha}}}{18 L_\alpha \mu_a} \tag{4}$$

Here $\boldsymbol{u_a}, \boldsymbol{g}, \rho_a, \rho_d$ represent the velocity component of air, the gravity force, and the density of air and water, respectively. L_α, μ_a represents the characteristic length and viscosity of air, respectively. The first, second, and third terms on the right-hand side of the equation (2) represent the drag force on the droplets, the buoyancy force from gravity, and the forces exerted on an air particle that would have occupied the volume of the droplet, respectively. The local Froude number appearing in the second term is defined as

$$Fr = \frac{\parallel \boldsymbol{u_{a,\alpha}} \parallel}{\left(L_\alpha g\right)^{0.5}} \tag{5}$$

In most cases, the last term is negligible due to the low ratio of air-to-water densities. The empirical correlation used for drag coefficient of droplet C_D is as follows,

$$C_D = (24/Re_d)(1 + 0.15Re_d^{0.687}) \quad \text{for } Re_d \leq 1300$$
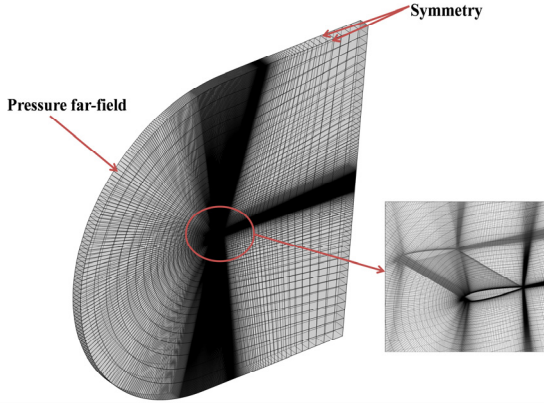$$C_D = 0.4 \qquad \text{for } Re_d > 1300 \tag{6}$$

Fig. 1 Computational domain and spatial discretization

The non-dimensional air velocity $\boldsymbol{u_a}$ is obtained from the Navier-Stokes-Fourier equations. Due to low liquid water concentration, the effect of the droplets on the airflow is neglected.

Water volume fraction and droplet velocity vector in whole domain can be evaluated by solving the equations (1) and (2). Then, the collection efficiency, β, can be easily determined by the following relation($\boldsymbol{n}$ being the unit vector normal to the solid surface):

$$\beta = -\alpha \boldsymbol{u_d} \cdot \boldsymbol{n} \tag{7}$$

The computational domain and grid distribution of an airfoil together with boundary conditions are illustrated in Fig. 1. A grid generation tool, GAMBIT, and an ice accretion solver, ICE3D module of FENSAP-ICE[15] are used. The ICE3D module is conceptually based on the Messinger model[16] and is capable of predicting water runback on the surface. In implementing this partial differential equation approach, a simple assumption of taking a linear profile for the water film velocity $\boldsymbol{u_f}(X,y)$ with a zero velocity at wall is used,

$$\boldsymbol{u_f}(X,y) = \frac{y}{\mu_w} \boldsymbol{\tau}_{wall}(x) \tag{8}$$

where $\boldsymbol{\tau}_w$, the shear stress from the air, is the main driving force for the water film. A mean water film velocity is then obtained by averaging the thickness of the film h_f,

$$\overline{\boldsymbol{u_f}}(x) = \frac{1}{h_f} \int_0^{h_f} \boldsymbol{u_f}(X,y)dy = \frac{h_f}{2\mu_w} \boldsymbol{\tau}_{wall}(x) \tag{9}$$

Now, the mass conservation equation[17] can be written as follows,

$$\mu_w \left[\frac{\partial h_f}{\partial t} + \nabla \cdot (\overline{\boldsymbol{u_f}} h_f) \right] = U_\infty LWC\beta - \dot{m}_{evap} - \dot{m}_{ice} \tag{10}$$

where $U_\infty LWC\beta$ represents the mass transfer by water droplet impingement, $\dot{m}_{evap}$ represents evaporation, $\dot{m}_{ice}$ represents ice accretion. The energy conservation[17] equation can be written as follows,

$$\rho_w \left[\frac{\partial h_f C_w T}{\partial t} + (\overline{\boldsymbol{u}}_f h_f C_w T) \right]$$
$$= \left[C_w T_{d,\infty} + \frac{\| \boldsymbol{u}_d \|^2}{2} \right] \times U_\infty LWC\beta \tag{11}$$
$$- 0.5(L_{evap} + L_{subl})\dot{m}_{evap} + (L_{fusion} - C_{ice}T)\dot{m}_{ice}$$
$$+ \sigma\big((T_\infty + 273.15)^4 - (T + 273.15)^4\big) + \dot{Q}_h$$

Here, $\left[C_w T_{d,\infty} + \dfrac{\| \boldsymbol{u}_d \|^2}{2} \right] \times U_\infty LWC\beta$ represents the heat transfer caused by the supercooled water droplets impinging on the surface, $0.5(L_{evap} + L_{subl})\dot{m}_{evap}$ represents the heat transfer caused by evaporation, and $(L_{fusion} - C_{ice}T)\dot{m}_{ice}$ represents the heat transfer caused by ice accretion. The radiative and convective heat transfer terms are represented as $\sigma((T_\infty + 273.15)^4 - (T + 273.15)^4)$, and $\dot{Q}_h$, respectively.

The heat flux obtained from the air flow solution is converted into a heat transfer coefficient prior to ice accretion calculation. The coefficients ρ_w, C_w, C_{ice}, L_{evp}, L_{subi}, and L_{fusion} represent the density of water, the specific heat capacity of water and ice, the latent heat of evaporation, the latent heat of sublimation, and the latent heat of fusion, respectively. The airflow and droplet parameters $T_{d,\infty}$, U_∞, LWC and T_∞ are specified by the user input.

The collection efficiency, β, and the droplet impact velocity, $\boldsymbol{u}_f$, are provided by the Eulerian droplet solver. The air flow solver provides the convective heat flux, $\dot{Q}_h$, and the local wall shear stress, $\boldsymbol{\tau}_{wall}$. Then, the three unknowns, the equilibrium temperature T, the film thickness h_f and the mass of accreted ice $\dot{m}_{ice}$ can be determined using the equations (10) and (11). In order to close the system, the following compatibility relations are
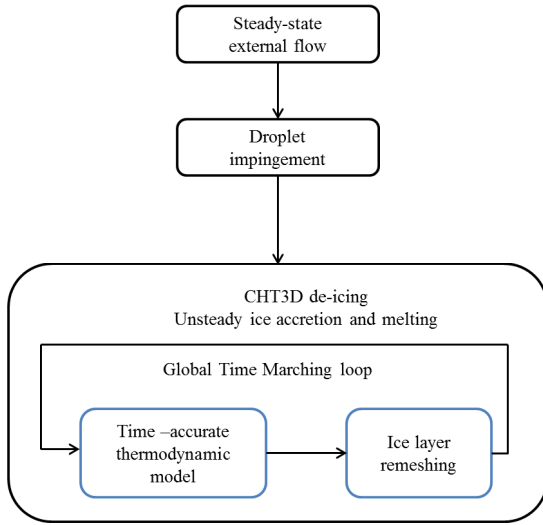
Fig. 2 Flowchart of unsteady conjugate heat transfer

used;

$$h_f \geq 0 \qquad (12)$$

$$\dot{m}_{ice} \geq 0 \qquad (13)$$

$$h_f T \geq 0 \qquad (14)$$

$$\dot{m}_{ice} T \leq 0 \qquad (15)$$

A cell-centered finite volume method is used to discretize these equations.

Finally, the melting process in the ice layer and the heat conduction through the solid layers are evaluated by the 3D heat conduction module CHT3D. The nonlinear unsteady heat conduction equation for each material can be expressed as,

$$\frac{\partial H_M(T)}{\partial t} = \nabla \cdot (k_M(T) \nabla T) + S_M(t) \qquad (16)$$

where $H_M(T)$ and $k_M(T)$ are the enthalpy and the conductivity of material M, respectively, and depend on the varying local temperature T. In order to describe the effects of electric heaters, a volumetric heat source term, $S_M(t)$, has been introduced in the equation. The user can change the heater power through a control sequence or by using a thermostat to confine the temperature within certain limits. A canonical Galerkin finite element discretization is used to solve the equation and the implicit backward Euler scheme is used for time integration.

The unsteady conjugate heat transfer module(CHT3D) is used for de-icing simulations[18]. This module requires the time accurate solution of mass, momentum and energy balance between air and water flows, water film, and ice layer. The air solution computed by Navier-Stokes-Fourier equations is set the initial solution and, with water mass collected on the exposed surfaces, the CHT3D module can be initiated. In the CHT3D loop, at each time step, Newton iterations are performed until the heat fluxes are conserved. Then, based on the net mass growth from the film and shrinkage due to melting, the ice shape can be computed. The flow chart of unsteady CHT3D simulation is shown in Fig. 2.

Electro-thermal ice protection systems are typically built with multi-layer and multi-material skin assemblies divided into separate heating strips. The simulations of these arrangements usually involve a single-fluid domain. Initial solutions are required for droplet and surface liquid water film. These solutions should be set up with a specified wall temperature on the interface so that the initial non-zero wall heat fluxes may ensure good convergence.

3. Calculation of Heater Properties

In de-icing analysis of a wing surface or wind turbine blade, heater parameters such as heater length, heater area and power requirement for de-icing have to be calculated prior to the modeling of blade(or wing). Generally, ice accumulates along the leading edge of the blade; therefore the heater should be large enough that the leading edge may be covered. For the current analysis, the heater area is chosen based on a representative geometry of a cylinder at the leading edge with a diameter equal to a quarter of the blade thickness, followed by a section that is one quarter of the length of the chord. The length of the heater from the leading edge is calculated[19] as:

$$L_h = \frac{\pi}{16} t + \frac{1}{4} C \qquad (17)$$

where t is the chord thickness and C is the chord length. In order to reduce the complexity, it is assumed that the heater length is equal on both of the bottom and the top. The total area A is calculated by multiplying the total length of the heater by the span width. At different angles of attack, the ice accumulation area will change, depending on the droplet impingement. Higher angles of
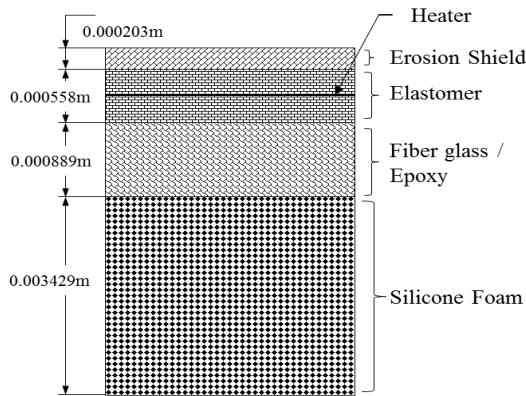
Fig. 3 Material composition of leading edge

attack will result in a wider accumulation of ice on the pressure side of the airfoil. On the contrary, negative angles of attack will result in more ice accumulation on the suction side of the airfoil. Moreover, the trailing edge of the airfoil may need to be protected in the event of run-back icing.

The power of the heating elements installed on the airfoil surface depends on the convective heat transfer coefficient h_1, the ambient, target, and surface temperatures T_{amb}, T_C, T_h, and the heating area A. It can be mathematically expressed as

$$P(t) = h_1 A(T_{amb} - T_C) + h_1 A(T_C - T_h) \qquad (18)$$

The first term on the right-hand side represents an approximation of the power required for the de-icing and the second one represents the correction, considering the gap between the target and surface temperatures. The heating coefficient h_1 may be approximated with the convective heat transfer coefficient, evaluated based on a flat plate hypothesis given by

$$h_1 = \rho_{air}.C_{p_{air}}.U_\alpha.St \qquad (19)$$

Here the Stanton number St, the friction coefficient, and the Reynolds number Re are defined as

Table 1 Heater parameters for DU21 airfoil

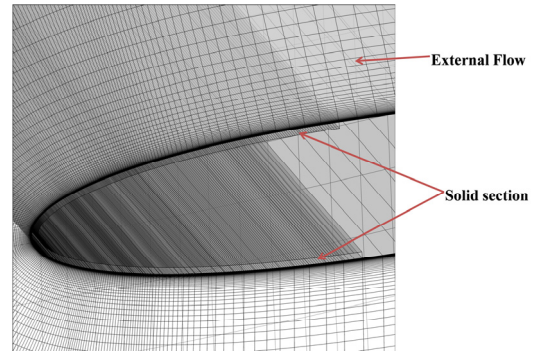| Ambient temperature(K)	263.15
Surface temperature(K)	273.15
Length of heater(m)	1.0199
Heating power(W/m²)	4313.7

Fig. 4 Computational domain with solid section

$$St = \frac{1}{2}c_f, \quad c_f = \frac{0.058}{Re^{0.2}}, \quad Re = \frac{\rho_{air}.U_\alpha.c}{\mu_{air}} \qquad (20)$$

Since heating elements are located in the turbulent zone of the airfoil, the turbulent friction coefficient c_f is used.

The wind turbine blade selected for current analysis is DU21 and it is one of the airfoil sections of NREL 5MW wind turbine[20,21]. The target temperature is assumed to be 288 K and all heater parameters are described in Table 1. The calculated heater geometrical parameters(heater length and area) are used to model the heater and the calculated heater power requirement is used in FENSAP for the current computational model.

4. Results and Discussions

The NASA Lewis Research Center conducted experiments on thermal ice protection system for NACA0012 airfoil with a chord of 0.9144 m and span of 1.8288 m[22]. The model was fabricated into two pieces: a leading edge section(0.224 m) of chord, and a wooden after-body(0.6604 m). The leading edge material composition and thickness information are given in Fig. 3.

The material property of each layer is illustrated in Table 2. The computation domain of leading edge heater section with external flow domain is shown in Fig. 4. The

Table 2 Leading edge material properties

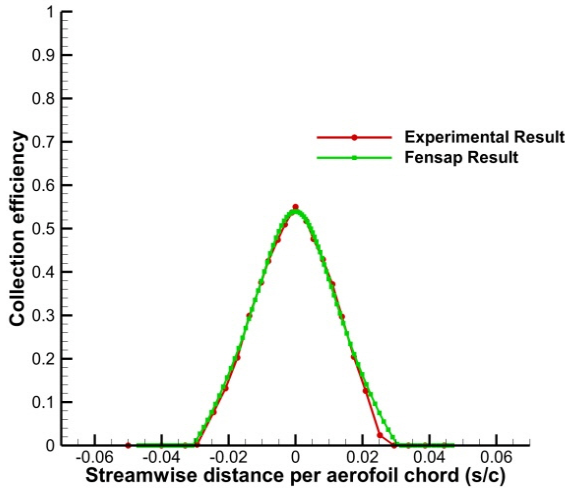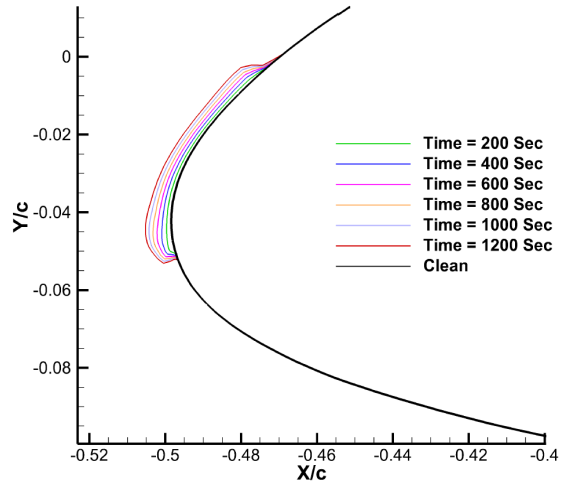| Material Name	Density Kg/m³	Conductivity w/m·k	Enthalpy J/kg
Erosion shield	8025.3	16.250	137,235
Elastomer	1383.9	0.2561	343,087
Fiberglass /epoxy	1794.0	0.2940	428,859
Silicone Foam	648.75	0.1210	308,779

Fig. 5 Comparison of collection efficiency

Fig. 7 Ice accretion at various time intervals on DU21 airfoil without IPS
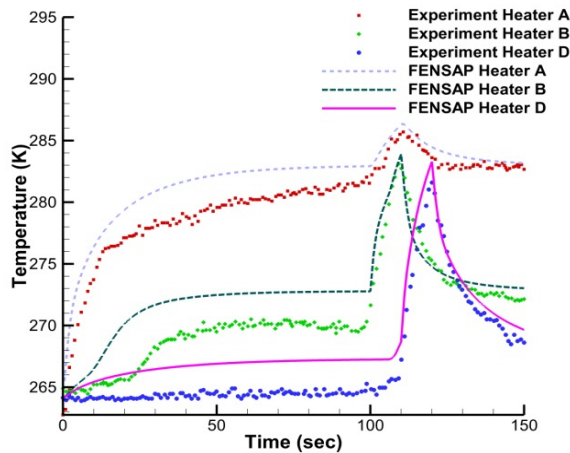

Fig. 6 Comparison of first heater temperature for NACA 0012

boundary conditions applied for the current study is shown in Table 3.

Accurate air-flow solution around the NACA0012 airfoil is predicted by the finite volume Navier-Stokes-Fourier code. The collection efficiency results are shown in Fig. 5 and turn out to be in good agreement with the experimental data. The collection efficiency shows the potential of ice formation on the exposed surface.

Seven heating elements operated in a sequence for 600 seconds are used for validating the de-icing computational model. The seven heaters were named as A-G and the heater sequence as well as sequence of heater activation were chosen to be same as experiment[22]. The comparison of heater temperature is shown in Fig. 6.

The results compare reasonably well to the experimental data, which explicitly shows the correct implementation of heating elements and this computational model can be applicable for other flow conditions. On the other hand, the cooling cycle of heater B did not match properly with the experimental data. This result may be related to limitations of thermal and runback water models of FENSAP.

The computational model was also applied to the DU21 airfoil the same as NACA0012 but with different boundary conditions as shown in Table 3. Fig. 7 illustrates the shapes of ice accretion on the DU21 airfoil for various icing exposure times with a maximum exposure time of 1,200 seconds.

It is apparent that the ice formed on the surface of the airfoil disturbs the flow and changes the flow field which may affect the performance of wind turbine. IPS can be an option to avoid the performance degradation under this flow conditions. Heater parameters calculated in section 3 is used to model the heater and the heater power input in

Table 3 Boundary conditions

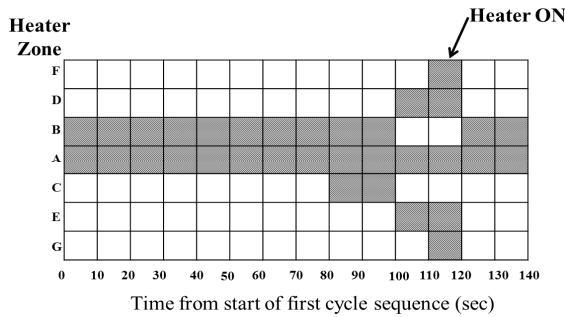|	NACA0012	DU21
Velocity(m/s)	44	66.48
Temperature(K)	266.48	263.15
LWC(g/m^3)	0.78	0.38
Heater A(W/m^2)	7750.1	4313.7
Heater B,C(W/m^2)	10850	4313.7
Heater D-G(W/m^2)	10850	4313.7

Fig. 8 Typical heater cycle sequence for DU21 airfoil
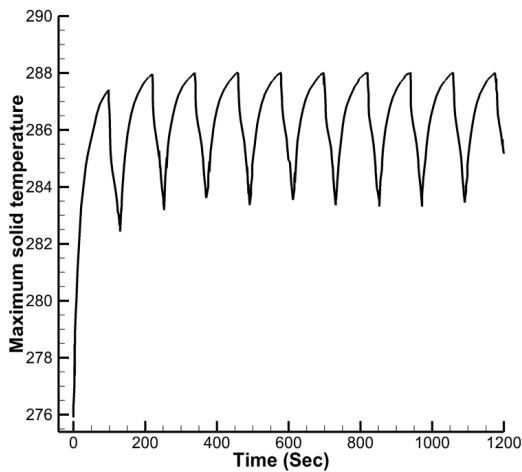
Fig. 9 Time variations of solid surface temperature on DU21 airfoil

Fig. 10 Ice accretion at various time intervals with IPS for DU21 airfoil
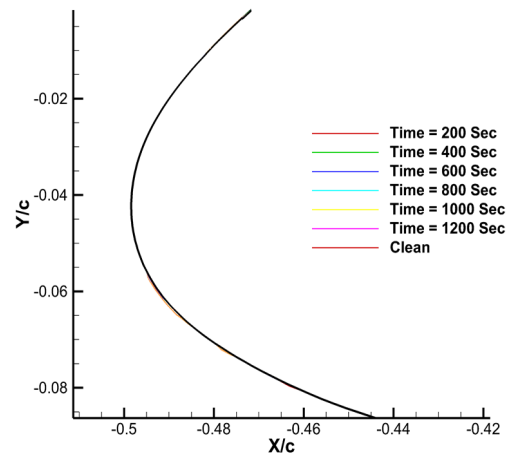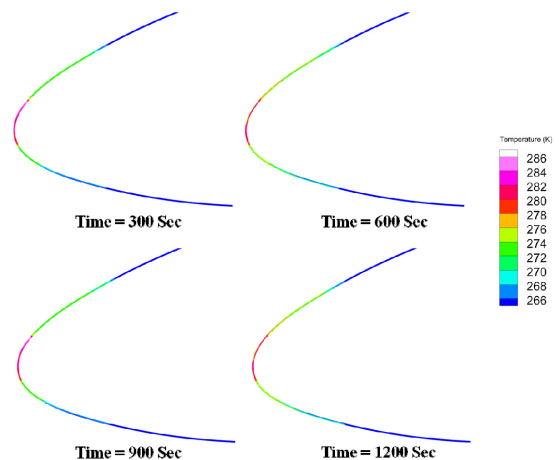

Fig. 11 Temperature distributions at solid section at various time intervals for DU21 airfoil

FENSAP. The material property and composition of the leading edge for the current model is chosen to be the same as NACA0012. Since the angle of attack and the type of airfoil are different, the heater cycle and heater sequence are changed for the current simulation. The seven heaters named as A-G and, in the first cycle, heaters A and B are activated for 80 seconds. The heaters A, B and C are then activated in the second cycle for 20 seconds. Followed by this, the heaters A, D, E, F and G are activated in the third cycle for 10 seconds. The sequence of the operation of heaters are illustrated in detail in Fig. 8.

The maximum solid surface temperature on the airfoil is shown in Fig. 9. The trend shown in the DU21 surface temperature remains the same as NACA0012 surface temperature. The maximum temperature on the surface of airfoil does not exceed very much above 288 K. This

indicates that the heater parameter calculations in section 3 are acceptable. The ice accretion results at various time steps with IPS are also shown in Fig. 10. Shedding of ice and dramatic reduction of ice accretion can be easily observed.

The contours of temperature at solid section at various time intervals for DU21 airfoil are shown in Fig. 11. The propagation of heat during time steps is explicitly shown in these figures. The results of DU21 airfoil with IPS are acceptable and consequently the same methodology may be applicable for other airfoil sections of NREL 5MW or any other wind turbines.

5. Conclusion

In this study, performance of an electro-thermal ice protection system of aircraft and wind turbines in atmospheric icing conditions was investigated. The computational methods based on partial differential equations were used for the analysis of air flow, droplet impingement, ice accretion, conjugate heat transfer, and thermal ice protection systems.

In order to validate the computational model, an electro-thermal ice protection system installed at the leading edge of NACA 0012 airfoil was analyzed. It turned out that the present computational results, in particular, conjugate heat transfer predictions compare reasonably with experimental data in most cases. Nonetheless, some deviations were found in cooling cycle of heater. These discrepancies might be due to limitations of thermal and runback water models used in the code. Moreover, the same computational model was applied to the DU21 airfoil section of NREL 5MW wind turbine with calculated heater parameters. The general results and the heater parameter calculations turned out to be in acceptable range. Despite some discrepancies, this method can be used for industrial design applications like the minimization of power consumption while avoiding ridges on the upper surface of the wing in aircraft and the blade of wind turbines.

Acknowledgements

References

[1] 2000, Gent, R.W., Dart, N.P. and Cansdale, J.T., "Aircraft Icing," *Philosophical Transactions of the Royal Society A*, Vol.358, No.1776, pp.2873-2911.

[2] 1998, Kind, R.J., Potapczuk, M.G., Feo, A., Golia, C. and Shah, A.D., "Experimental and Computational Simulation of In-flight Icing Phenomena," *Progress in Aerospace Science*, Vol.34, No.5-6, pp.257-345.

[3] 2010, Jung, S.K., Myong, R.S. and Cho, T.H., "An Eulerian-Based Droplet Impingement and Ice Accretion Code for Aircraft Icing Prediction," *Journal of Computational Fluids Engineering*, Vol.15, No.2, pp.71-78.

[4] 2013, Jung, K.Y., Jung, S.K. and Myong, R.S., "A Three-Dimensional Unstructured Finite Volume Method for Analysis of Droplet Impingement in Icing," *Journal of Computational Fluids Engineering*, Vol.18, No.2, pp.41-49.

[5] 2013, Jung, S.K. and Myong, R.S., "A Second-Order Positivity-Preserving Finite Volume Upwind Scheme for Air-Mixed Droplet Flow in Atmospheric Icing," *Computers & Fluids*, Vol.86, pp.459-469.

[6] 2015, Ahn, G.B., Jung, K.Y., Myong, R.S., Shin, H.B. and Habashi, W.G., "Numerical and Experimental Investigation of Ice Accretion on a Rotorcraft Engine Air Intake," *Journal of Aircraft*, Vol.52, No.3, pp.903-909.

[7] 2015, Son, C.K., Oh, S.J. and Yee, K.J., "Development of 2nd Generation Ice Accretion Analysis Program for Handling General 3-D Geometries," *Journal of Computational Fluids Engineering*, Vol.20, No.2, pp.23-36.

[8] 2012, Villalpando, F., Reggio, M. and Ilinca, A., "Numerical Study of Flow around Iced Wind Turbine Airfoil," *Engineering Applications of Computational Fluid Mechanics*, Vol.6, No.1, pp.39-45.

[9] 2011, Parent, O. and Ilinca, A., "Anti-icing and De-icing Techniques for Wind Turbines: Critical Review," *Cold Regions Science and Technology*, Vol.65, pp.88-96.

[10] 2010, Barber, S., Wang, Y., Jafari, S., Chokani, N. and Abhari, R.S., "The Impact of Ice Formation on Wind Turbine Performance and Aerodynamics," *European Wind Energy Conference*.

[11] 1992, Yaslik, A.D., De Witt, K.J., Keith, T.G. and Boronow, W., "Three-Dimensional Simulation of Electro-Thermal Deicing Systems," *Journal of Aircraft*, Vol.29, No.6, pp.1035-1042.

[12] 1996, Thomas, S.K., Cassoni, R.P. and MacArthur, C.D., "Aircraft Anti-Icing and De-Icing Techniques and Modeling," *Journal of Aircraft*, Vol.33, No.5, pp.841-854.

[13] 2014, NTI Solutions User Manual, Newmerical Technologies Inc.

[14] 2001, Beaugendre, H., Morency, F. and Habashi, W.G. "ICE3D, FENSAP-ICE's 3D In-flight Ice Accretion Module," *8th Aerodynamics Symposium*, CASI, Toronto.

[15] 2000, Bourgault, Y., Boutanios, Z. and Habashi, W.G., "Three-Dimensional Eulerian Approach to Droplet

Impingement Simulation Using FENSAP-ICE, Part 1: Model, Algorithm, and Validation," *Journal of Aircraft*, Vol.37, No.1, pp.95-103.

[16] 1953, Messinger, B.L., "Equilibrium Temperature of an Unheated Icing Surface as a Function of Air Speed," *Journal of the Aeronautical Sciences*, Vol.20, pp.29-42.

[17] 2003, Beaugendre, H., Morency, F. and Habashi, W.G., "FENSAP-ICE's Three-Dimensional In-Flight Ice Accretion Module: ICE3D," *Journal of Aircraft*, Vol.40, No.2, pp.239-247.

[18] 2002, Croce, G., Beaugendre, H. and Habashi, W.G., "CHT3D, FENSAP-ICE Conjugate Heat Transfer Computations with Droplet Impingement and Runback Effects," *AIAA Paper 2002-7212*.

[19] 2014, Suke, P., "Analysis of Heating Systems to Mitigate Ice Accretion on Wind Turbine Blades," *Master Thesis*, McMaster University.

[20] 2013, Myong, R.S., "Atmospheric Icing Effects on Aerodynamics of Wind Turbine Blade," *ASME 2013 International Mechanical Engineering Congress and Exposition*.

[21] 2009, Butterfield, S., Musial, W. and Scott, G., "Definition of a 5-MW Reference Wind Turbine for Offshore System Development," *National Renewable Energy Laboratory*, US.

[22] 1997, Wright, W.B., Al-Khalil, K. and Miller, D., "Validation of NASA Thermal Ice Protection Computer Codes Part 2‐LEWICE/Thermal," *AIAA Paper 97-0049*.